A Novel Design Approach for a 60 GHz Circularly Polarized EBG Antenna

Taieb Elkarkraoui[1, *], Nadir Hakem[2], Gilles Y. Delisle[1], and Yacouba Coulibaly[2]

Abstract—This article focuses on the development of a high gain, broadband, circularly polarized Electromagnetic Band Gap (EBG) antenna operating at 60 GHz. The designed antenna is configured with a superstrate based on a frequency selective surface (FSS) placed in front of a cross dielectric resonator antenna (XDRA), installed into a ground plane, which acts as an excitation source. A fast Leaky-Wave approach based on transverse equivalent network (TEN) is used to deduce analytical radiation patterns formulas of the proposed antenna. The proposed analytical model was implemented and verified by a comparison with both numerical and experimental results. The reported results showed very satisfactory performances with an achievable impedance bandwidth ($S_{11} < -10$ dB) of 11.7% from 56 to 63 GHz, an axial-ratio bandwidth (AR < 3 dB) of 5.4% from 58.9 to 62.1 GHz and a stable gain of 16.7 dBi within the passband. A good agreement among analytical, numerical and measured results is successfully achieved and falls well within initially set specifications.

1. INTRODUCTION

In consumer, industrial and automotive areas, the demand for high-speed multimedia data communications, such as real-time video streaming file and geolocation data, is significantly increasing with time. Wireless data rates at microwave frequencies and below are currently limited to a data rate about 1 Gb/s. Therefore, one of the most obvious ways to achieve a wireless connection at a multi-gigabits rate is to use signals at millimetric wavelengths that supports high data rates which can be extended up to 10 Gb/s [1]. However, it is known that 60 GHz signals do not propagate well through obstructions since reflected and diffracted components are significantly attenuated. The polarization of the transmit antenna has a significant impact on the characteristics of reflected waves. Generally an antenna can receive either right-hand (RHCP) or left-hand circular polarization (LHCP) but significantly attenuates in the other polarization. Further, the "handiness" of the polarization can switch when a circularly polarized signal is reflected on the metalor concrete objects. This means that some multipath components could be significantly attenuated by the receive antenna. Transmitting a circularly polarized signal is a good solution to reduce multipath effects in line-of-sight (LOS) environments in the 60 GHz band [2].

Another major disadvantage of 60 GHz millimeter-wave is that oxygen absorption and propagation losses have significant impact which cannot be neglected [3]. These situations limit the communication achievable distance link, and overcoming these disadvantages requires a Circular Polarized (CP) high gain antennas.

A dielectric resonator antenna (DRA) [4] is very interesting for millimeter wave wireless communications because of its favorable characteristics, such as dimensions, compact structure, low cost, high yield and the ability to support a multitude of excitation systems. Although DRA also

has several drawbacks such as low gain and limited bandwidth, various gain enhancement methods of DRA have been reported such as using an antenna array [5], a superstrate structure [6], or using short horns around DRA [7]. The requirement to use circularly polarized antennas to obtain the required performances is linked to the fact that the techniques for a circular polarized DRA are still limited. In the public literature, many feeding techniques have been proposed to achieve circular polarization [8] such as exciting the DRA with a dual-coaxial probe, dual-conformal strip or with parasitic strips, rotated sequential and aperture feeds. So far there was a number of different element configurations published, including semi-elliptical DR with a hollow elliptical cylinder [9], radiating with a stair-shaped DR [10] and feeding with a square spiral strip [11]. Although most of the configurations mentioned show good performance to generate circular polarization, achievable gain and bandwidth are still below the objectives for the 60 GHz millimeter wave band.

In this paper, a novel hybrid approach is introduced to fulfill the requirements put on the fundamental parameters, such as gain and bandwidth, which uses the concept of EBG superstrate. Furthermore, a circular polarization radiation is generated by exciting the EBG structure with a cross dielectric resonator antenna (XDRA). The proposed antenna yields simultaneous advantages, namely high gain, large bandwidth and improved boresight axial ratio over the operating band. Furthermore, it is also characterized by a simple to achieve structure and easy integration.

In the following sections, first, the details of the proposed CP design are fully described. After that, the approach used to formulate radiation characteristics of a proposed antenna is extended. And finally, the analytical, numerical and measured results are presented and discussed in view of the design requirements.

2. ANTENNA DESIGN

2.1. Antenna Configuration

The proposed antenna which is considered as a Fabry-Perot resonator (FP) [12] is configured with an XDRA located at the center of the ground plane and covered with an FSS superstrate. Figure 1 presents a 3D view of this novel antenna structure.
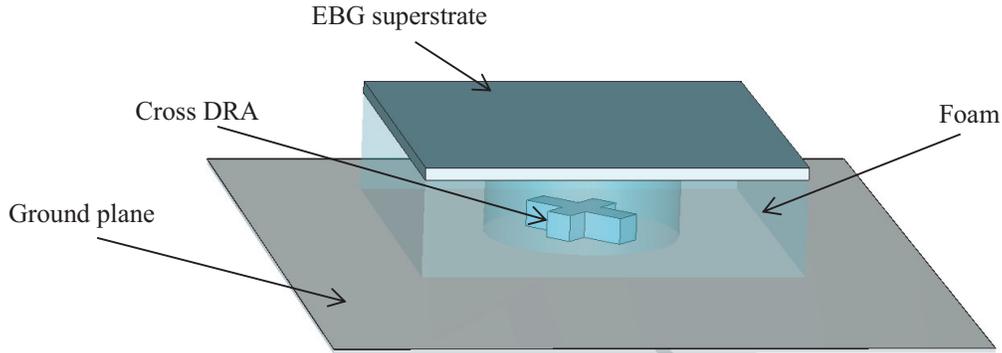

Figure 1. Antenna configuration.

To achieve an operational design at 60 GHz, the FP cavity is excited by an XDRA with dimensions of $L_c = 3.5$ mm, $W_c = 2.4$ mm and thickness of $h_c = 1.27$ mm (see Figure 2(b)). The cross is oriented at 45 degrees to an aperture coupling slot. A 50 Ω center fed microstrip line having a width $W_{\text{feed}} = 0.45$ mm and length $L_{\text{feed}} = 15$ mm is used to excite the cross dielectric resonator through the narrow rectangular slot having a length $L_s = 1$ mm and width $W_s = 0.2$ mm. A tuning stub with length $p = 1$ mm is added to the end of the microstrip line to optimize the matching of the antenna, and the dielectric substrate of the microstrip line has a width 20 mm, dielectric constant $\varepsilon_r = 2.2$ and thickness $h = 0.127$ mm. A square EBG superstrate of width $L_{\text{sup}} = 14$ mm, permittivity $\varepsilon_r = 10.2$ and loss tangent $\tan \delta = 0.003$ is placed at a distance $d_s = 2.5$ mm of the ground plane. In addition, printed patches (see Figure 2(a))

are placed on the lower side of the EBG superstrate. A Rohacell foam layer of thickness 2.5 mm and permittivity 1.07 is added between the ground plane and EBG superstrate to serve as support.

The design parameter values of the proposed 60 GHz EBG antenna of Figure 2 are given in Table 1. It should be noted that these values are not the sole possible set of acceptable values. The determinations of these values are empirical and must be based on a detailed understanding of the behavior of each of the antenna components.
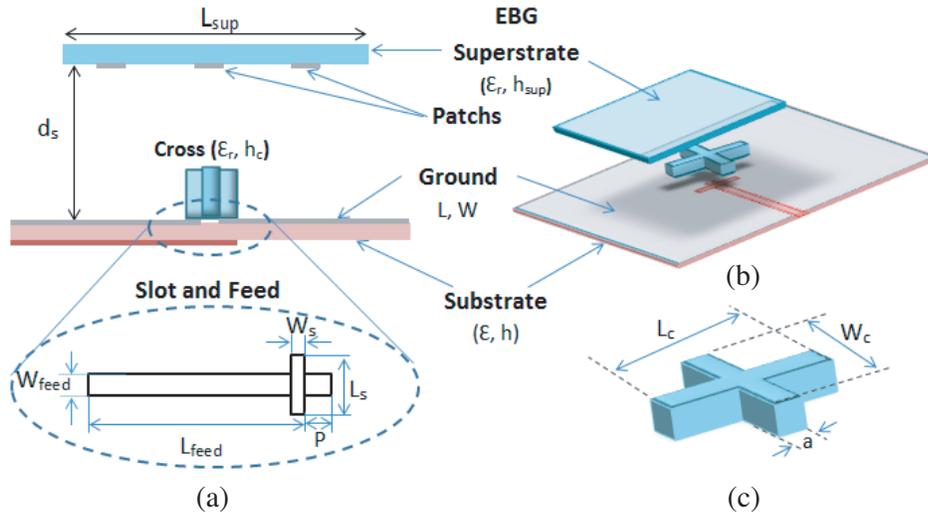

Figure 2. Antenna configuration: (a) Side view, (b) dimensions of the XDRA, (c) 3D view.

Table 1. Geometrical parameters of the proposed antenna.

EBG superstrate	$L_{\text{sup}} = 14 \, \text{mm}$, $W_{\text{sup}} = 14 \, \text{mm}$, $h_{\text{sup}} = 0.381 \, \text{mm}$, $d_s = 2.5 \, \text{mm}$
Cross Dielectric resonators.	$L_c = 3.5 \, \text{mm}$, $W_c = 2.4 \, \text{mm}$, $a = 0.86 \, \text{mm}$, $h_c = 1.2 \, \text{mm}$.
Slot	$L_s = 1 \, \text{mm}$, $W_s = 0.2 \, \text{mm}$
Substrate	$L = 25 \, \text{mm}$, $W = 20 \, \text{mm}$, $h = 0.127 \, \text{mm}$
Fed microstrip line	$L_{\text{feed}} = 15 \, \text{mm}$, $W_{\text{feed}} = 0.45 \, \text{mm}$

Normally, the design of an antenna EBG can be summarized in two major steps: firstly, the introduction of the excitation source having the most appropriate profile to achieve the desired final antenna and secondly, the involvement of the upper interface (superstrate) having required characteristics to achieve the desired gain on a predetermined operating band. The details of how the design of such an antenna can be accomplish are provided below.

2.2. Source of Excitation

First, the use of an excitation source will be discussed with the design method and the determination of an equivalent circuit. The excitation source should generate the same polarization as that of the final antenna.

From a conceptual viewpoint, the cross DRA is equivalent to the superposition of two rectangular resonators maintained orthogonal to each other. Therefore, the fabrication process for the cross DRA is simplified since the dedicated methods for a conventional rectangular DRA can be directly used.

The cross is positioned at a 45 degrees angle to an aperture coupling slot, allowing equi-amplitude excitation of the two arms of the cross. Each rectangular resonator transmits a linearly polarized wave in the boresight direction. To generate circularly polarized radiation from a linearly polarized DRA requires radiating two fields having equal (or nearly equal) amplitudes and being in phase quadrature,

which will give circular polarization when being combined [13, 14]. The geometry of the proposed source of excitation XDRA is optimized numerically so that the two arms of the cross radiate fields which are equal in amplitude (or near equal) and 90 degrees out of phase.

Figure 3 demonstrates a parametric study of the AR with different length to width ratios of the XDRA. The optimum AR ratio is found when the length to width ratio is 1.46 corresponding to the $L_c = 3.5\,\text{mm}$ and $W_c = 2.4\,\text{mm}$.
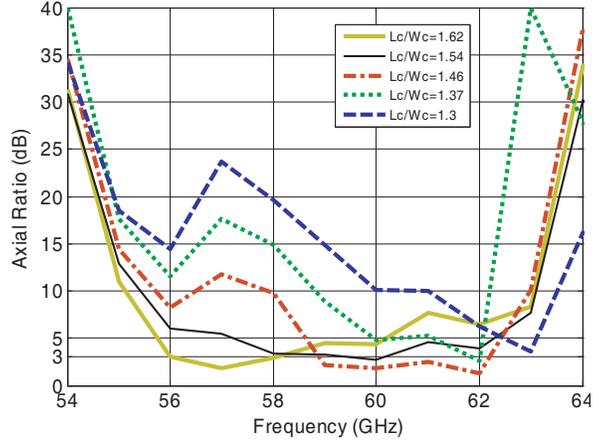

Figure 3. Axial ratio of the EBG antenna with different length to width ratios of XDRA.

An analytical study based on empirical equations for rectangular DRA has been done to estimate the resonant frequencies and factor of quality Q and exciting modes for each rectangular constituted the optimized XDRA. Some results obtained in this study are summarized in Table 2.

Table 2. Summary of analytical results.

	Rectangular 1		Rectangular 2	
Mode	Resonant frequency (GHz)	Q-factor	Resonant frequency (GHz)	Q-factor
$\text{TE}_{11\delta}$	58.4	2.66	60.1	3.58

It is then expected that by carefully adjusting the lengths of the two arms of the XDRA to be different and with a proper length ratio, two orthogonal TE_{11} modes are simultaneously excited, at two different frequencies: 58.4 GHz and 60.1 GHz, with equal amplitude (or near equal) and 90 degrees phase difference, thus circularly polarized radiation.

It will be noted that when the two rectangular resonators radiate nearly equal amplitude, we define the polarization to be nearly circular. By characterizing the radiation in terms of the axial ratio, to generate an ideal circularly polarized signal, this value must be equal to 0 dB. Generally, for circularly polarized signal, an axial ratio of less than or equal to 3 dB is considered as an appropriate value.

In the literature, various methods are available for the analysis of a coupled dielectric resonator antenna, namely the cavity model, transmission line model and hybrid approach. This contribution presents a simple approximate model based on the determination of the antenna input impedance [15–17]. First, the equivalent circuit of the structure is determined, and then, the constituent impedances of the circuit can be calculated.

The equivalent circuit of the microstrip-slot coupled cross dielectric resonator antenna is shown in Figure 4.

The XDRA is modeled by an admittance Y_{XDRA}, the slot modeled by admittance Y_{slot}, and the microstrip line, which ends with an open equivalent impedance circuit (stub) of length L_{stub}, modeled by Z_l. The coupling between the microstrip line and the slot is represented by the transformation ratio N.
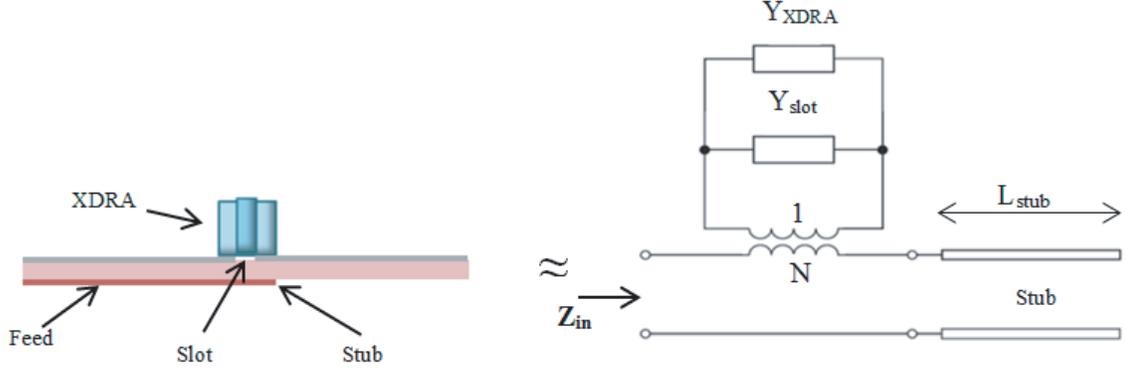
Figure 4. The equivalent circuit of the microstrip-slot coupled cross dielectric resonator antenna.

The first step is to model the cross dielectric resonator with an equivalent RLC network as shown in Figure 5.
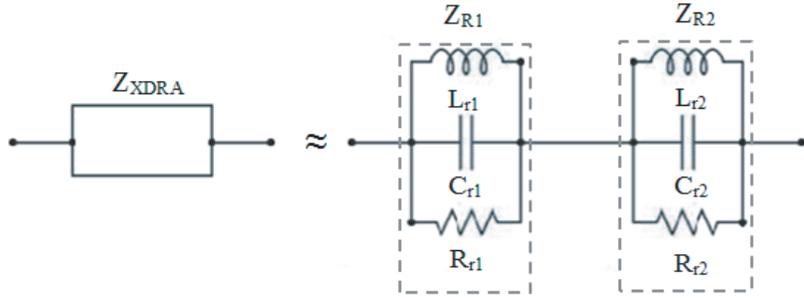

Figure 5. RLC equivalent parallel resonant circuit of the XDRA. Z_{R1} and Z_{R2} are the impedances of the two rectangular components of the cross dielectric resonator.

The impedance of XDRA is then given by:

$$Z_{\text{XDRA}} = Z_{R1} + Z_{R2} = \frac{1}{Y_{R1}} + \frac{1}{Y_{R2}} \tag{1}$$

By using the relations that can be found in [20, 21], the elements of RLC equivalent parallel resonant circuit of the resonator cross when being coupled to the excitation can be easily deduced.

$$R_r = \frac{2n^2 Z_0 s_{11}}{1 - s_{11}} \tag{2}$$

$$C_r = \frac{Q}{\omega_0 R_r} \tag{3}$$

$$L_r = \frac{1}{C_r \omega_0} \tag{4}$$

where S_{11} is the reflection coefficient, Z_0 the characteristic impedance, Q the quality factor calculated in the previous section, and n the coupling ratio between the DR and the excitation source.

The second step is to determine the input impedance of the slot. The rectangular slot in the ground plane can be modeled by two transmission lines, short-circuited to the length $L_s/2$. As a consequence, the admittance of the slot is expressed as:

$$Y_{\text{slot}} = -\frac{2j}{Z_c} \cot\left(\beta_f \frac{L_s}{2}\right) \tag{5}$$

where Z_c, β_f and L_s are respectively the characteristic impedance, wave number and length of the slot.

The last step involves modeling the microstrip line which ends with open equivalent impedance:

$$Z_l = -jZ_{cl}cot\left(\beta_l L_{\text{stub}}\right) \tag{6}$$

where Z_{cl} and β_l are the characteristic impedance and wave number of the line microstrip feed.

The input impedance Z_{in} of the structure shown in Figure 4 can be expressed as:

$$Z_{in} = \frac{N^2}{Y_{\text{XDRA}} + Y_{\text{slot}}} + Z_l \tag{7}$$

The transformation ratio N is given by the ratio between the discontinuity of the voltage on the line and the voltage on the slot assuming that the slot is thin; the following approximation can be used:

$$N = \frac{L_s}{\sqrt{W_{\text{feed}}h}} \tag{8}$$

where W_{feed} is the effective width of feed line and h the height of substrate. It should be noted that all equations previously cited from Eqs. (5) to (8) can be found in [15–19].

Once the geometry and equivalent circuit of the excitation source have been determined, we can pass to the choice of the EBG superstrate.

2.3. FSS Superstrate

The second phase of designing an EBG resonator antenna is the characterization of the upper interface. The structure which must assume the role of the partially reflective surface is designed to achieve a high gain and wide bandwidth.

The used FSS surface is composed of a 1D square patch with size $= 1.2\,\text{mm}$ and periodicity $p = 2\,\text{mm}$ (Figure 6). To determine the reflective properties of the studied structure, it is sufficient to illuminate one unit cell of this structure by a plane wave. The simulated reflection (S_{11}) and transmission (S_{21}) responses of the FSS superstrate unit cell are shown in Figure 7.
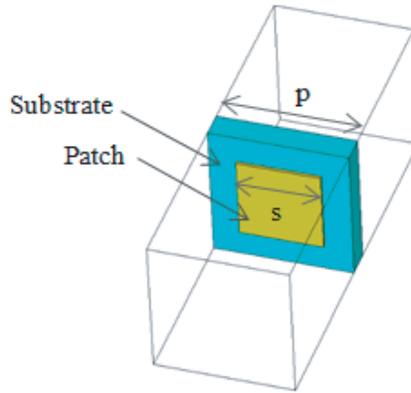

Figure 6. Dimension of the FSS superstrate unit cell.

The height of the proposed EBG antenna which is considered as a Fabry-Perot resonator can be calculated using the following equation [22].

$$d_s = \frac{c}{2f}\left(\frac{\Phi_{\text{FSS}} + \Phi_{\text{Gnd}}}{2\pi}\right) \tag{9}$$

where c is the velocity of light $3.10^8\,\text{m/s}$, f the operation frequency, Φ_{Gnd} the reflection phase of the lower interface, and Φ_{FSS} the reflection phase of the superior interface of the resonator. From Figure 7, at 61 GHz, the value Φ_{FSS} is 177°. As known, the ground plane is a perfect electric conductor; consequently, Φ_{Gnd} is equal to 180°. Using these phase values of the reflection coefficient, it becomes possible to calculate the height d_s of the EBG antenna cavity using Equation (9). d_s is found to be 2.44 mm and because of manufacturing constraints, this value is chosen to be 2.5 mm.
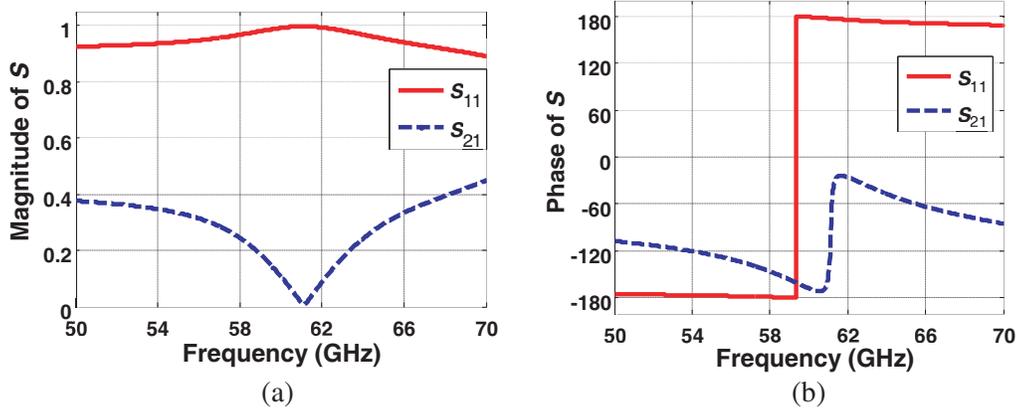
(a)   (b)

Figure 7. (a) Magnitude and (b) phase of reflection (S_{11}) and transmission (S_{21}) coefficients.

2.4. Simulations

With a suitable proposed design of the FSS superstrate placed at an adequate distance from a perfect electric ground plane, it is possible to improve the performance of XDRA in terms of bandwidth, gain, and efficiency.

The simulated voltage standing wave ratios (VSWR) of the XDRA is compared with that of XDRA with FSS superstrate in Figure 8(a). The matching frequency range of XDRA is found to be from 58.3 to 61.8 GHz (VSWR ≤ 2), corresponding to a bandwidth of 3.5 GHz (about 5.83% with center frequency at 60 GHz). The matching frequency range of the XDRA with superstrate is from 58.2 to 62.6 GHz (VSWR ≤ 2) corresponding to a bandwidth of 4.4 GHz (about 7.33% with center frequency at 60 GHz). The impedance bandwidth is therefore increased by 1.5%. It is expected that the bandwidth of the XDRA with FSS superstrate antenna will be higher than that of the XDRA only.
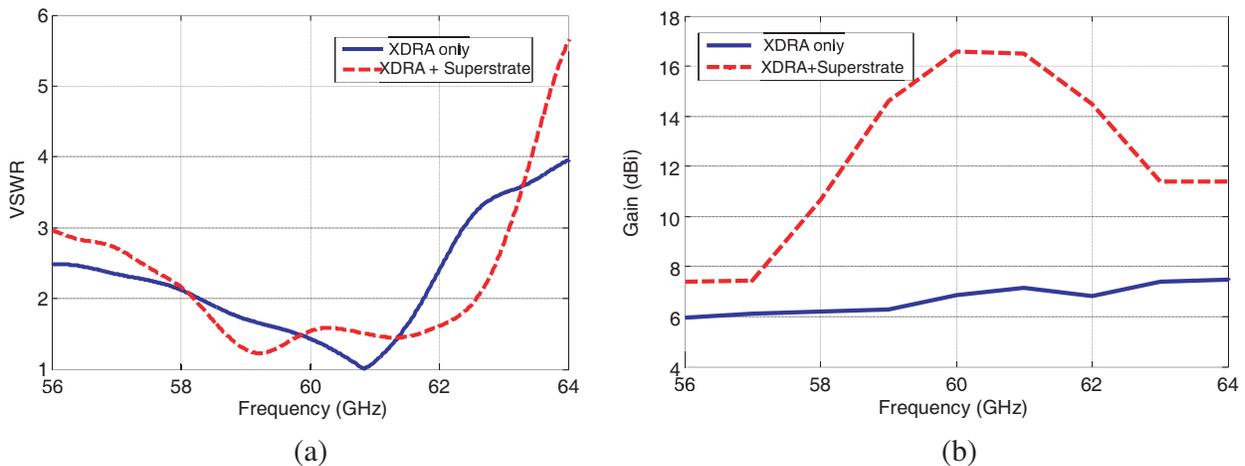

(a)   (b)

Figure 8. (a) Simulated bandwidth and (b) gain of the XDRA with and without the EBG.

The gain of the antenna with and without the FSS superstrate is calculated numerically using CST software and represented in Figure 8(b). It is noted that the gain increases from 6.9 dBi to about 16.7 dBi after adding the FSS superstrate.

It is confirmed that adding superstrate FSS above dielectric resonator antenna can improve gain and bandwidth. The bandwidth has been increased by 1.5%, while the gain has been enhanced by approximately 9.8 dBi.
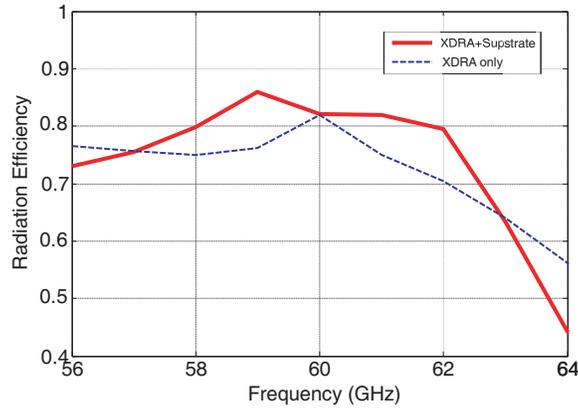
Figure 9. The radiation efficiency of the XDRA with and without the EBG.

The antenna radiation efficiency of XDRA with and without superstrate FSS is calculated numerically using CST software and represented in Figure 9. It can be noted from the results that the highest radiation efficiency ($\sim 85\%$) is obtained at 59 GHz. The radiation efficiency increases by approximately 10% at 59 GHz after adding the superstrate. The increased efficiency is considered to be a result of the increase in the antenna gain because of the direct proportionality between the gain and efficiency.

3. MODAL ANALYSIS OF THE EBG ANTENNA

In this section, a fast analytical solution for the far-field radiation of a dielectric resonator antenna covered with a FSS superstrate is introduced. The proposed analysis method is based on three consecutive steps. A self-explaining flowchart describing step-by-step the proposed analysis method is presented in Figure 10.
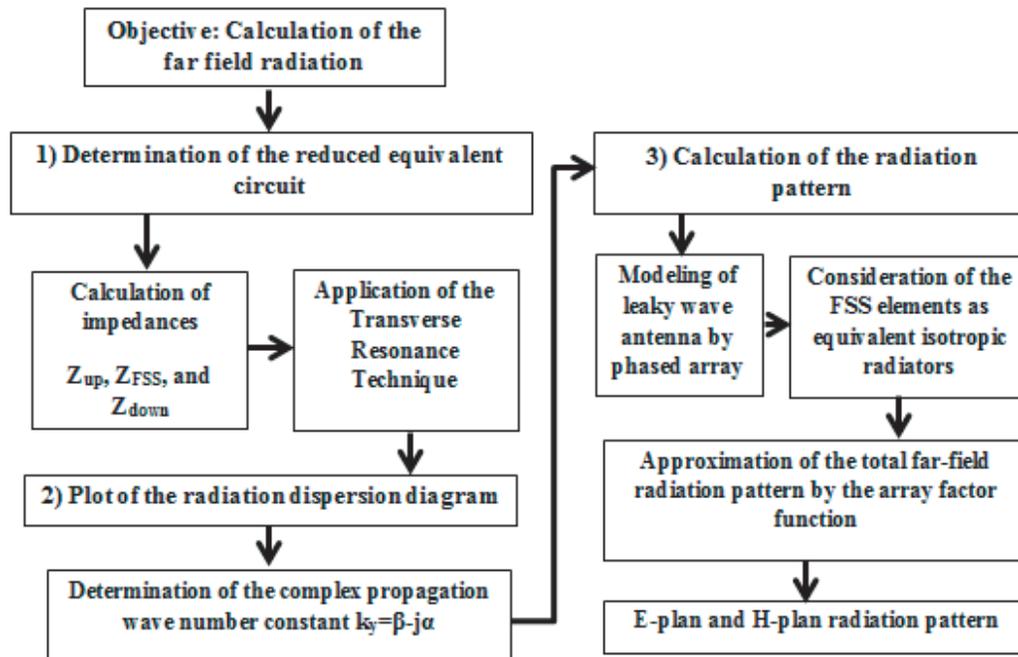

Figure 10. A flow chart explaining the analysis steps of the proposed method.

The modelling technique employed in this work is similar to the method of transverse equivalent network (TEN) used for the analysis of a leaky-wave antennas (LWA) [23, 24]. This method provides a quick way to predict the behaviour of the complex propagation wave number constant $k_y = \beta - j\alpha$ within the cavity where β stands for the propagation or phase constant, and α is the attenuation rate, due to the radiation or leakage induced by the LWA.

3.1. Reduced Equivalent Circuit

To analyze the cavities and deduce their radiating characteristics, the equivalent model of the transverse FP antenna is used and shown in Figure 11.
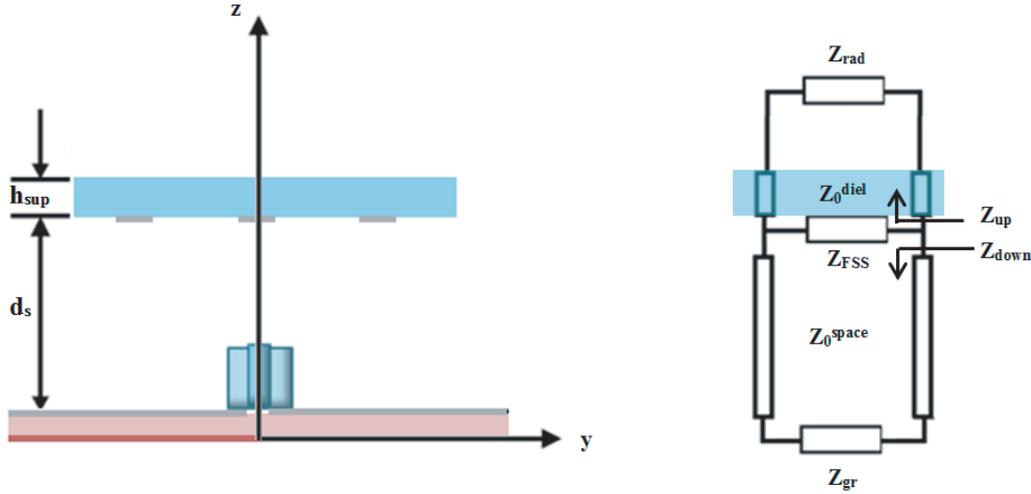

Figure 11. Equivalent Network of the proposed antenna.

The reduced equivalent circuit consists of three impedances [25]; the first one on top corresponds to the Z_{up}

$$Z_{\mathrm{up}} = Z_0 \frac{Z_{\mathrm{rad}} + jZ_0 \tan(k_z^{\mathrm{diel}} h_{\mathrm{sup}})}{Z_0 + jZ_{\mathrm{rad}} \tan(k_z^{\mathrm{diel}} h_{\mathrm{sup}})} \tag{10}$$

where Z_{rad} corresponds to the environment where the radiated energy propagates and expresses differently if dealing with TE or TM modes, for the case of free-space propagation:

$$Z_0^{TE} = \frac{\omega\mu_0}{k_z} \tag{11}$$

$$Z_0^{TM} = \frac{\omega\varepsilon_0}{k_z} \tag{12}$$

μ_0 is the permeability, ε_0 the permittivity, and η_0 the intrinsic impedance of free-space.

The second impedance considered in the equivalent circuit is the one corresponding to the frequency selective surface named Z_{FSS}. To calculate this impedance, a finite integration technique (FIT) [26] is used.

$$Z_{\mathrm{FSS}} = -\frac{Z_0^{\mathrm{diel}}(1 + \Gamma)}{2\Gamma} \tag{13}$$

where Γ is the reflection coefficient of the FSS layer.

The impedance represented at the bottom of Figure 11 corresponds to Z_{down}. Basically, it is the ground plane impedance transported to the second surface. Using the equivalent resonator modeling presented in the previous section, the equation of this translation of impedance can be easily calculated:

$$Z_{\mathrm{down}} = Z_0 \frac{Z_{gr} + jZ_0 \tan(k_z d_s)}{Z_0 + jZ_{gr} \tan(k_z d_s)} \tag{14}$$

Once all impedances have been calculated, the transverse resonance technique can be applied from the equivalent network of the total structure shown in Figure 11. When the TE polarization is considered, the transverse resonance technique function is expressed as follows:

$$Y_{\text{up}}(k_y) + Y^{\text{FSS}}(k_y) + Y_{\text{down}}(k_y) = 0 \tag{15}$$

It can be appreciated that each element included in the TEN is a function of k_y.

$$k_z^{\text{space}} = \sqrt{k_0^2 - k_y^2} \tag{16}$$

$$k_z^{\text{diel}} = \sqrt{k_0^2 \varepsilon_r - k_y^2} \tag{17}$$

3.2. Dispersion Diagram

The condition verified by Eq. (15) is used to determine and plot the radiation dispersion diagram of Figure 12, which demonstrates the evolution of the normalized phase β/k_0 and leakage constants α/k_0 with frequency. An approximate solution for this equation can be found with Newton-Raphson interpolation method for the phase and attenuation constants.
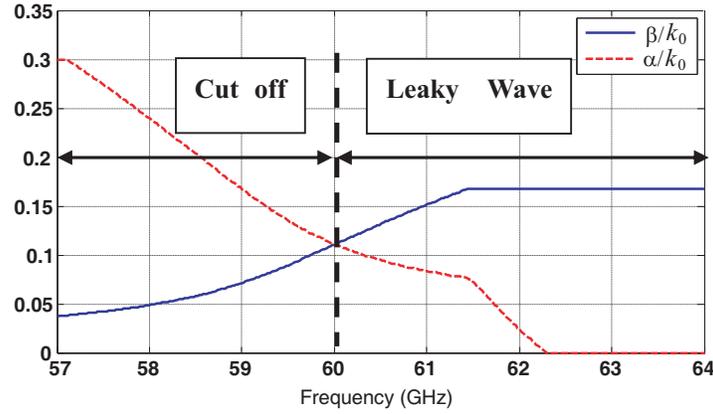

Figure 12. Normalized leaky-wave phase (β/k) and attenuation (α/k) constants as a function of frequency.

In our case (one dimensional LWA), the frequency which satisfies the relation $\beta = \alpha$ is defined as the cutoff leakage frequency at 60 GHz. The cutoff regime covers frequencies which satisfy $\beta < \alpha$, and the leaky wave mode starts propagating above the cutoff frequency. After the complex propagation wave number constant $k_y = \beta - j\alpha$ has been determined, one can calculate the radiation pattern.

3.3. Radiation Pattern

In order to obtain the radiation pattern for the structure shown in Figure 11, the leaky-wave antenna can be modeled as a phased array antenna composed of the same number of FSS unit cells along the y-axis of the wave propagation.

Figure 13 shows a LW antenna configured as a linear array fed continuously solely at one end of the structure with magnitude (I_n) and exponential phase (ξ_n) function.

The phase constant β, which determines the angle of the leaky wave antenna radiation θ in plane ZY, can be expressed by the formula:

$$\cos(\theta) = \frac{\beta}{k_0} \tag{18}$$

Noting that the unit cells of such structures are electrically small, the array factor approach demonstrated in [27] has been used. Under this approach, each FSS element was considered as a
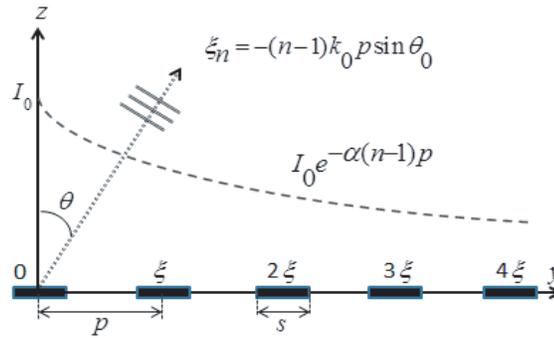
Figure 13. Array factor approach principle.

point source (isotropic radiator), fed with a current with magnitude $I_n = I_0 e^{-\alpha(n-1)p}$ and exponential phase $\xi_n = -(n-1)k_0 p \sin \theta_0$, where α is the attenuation constant calculated in Section 3.2. Then, the total far-field radiation pattern $R(\theta)$ is approximated by the array factor function:

$$R(\theta) = AF(\theta) = \sum_{n=1}^{N} I_n e^{j(n-1)k_0 p \sin \theta + j\xi_n} \tag{19}$$

where N represents the number of the FSS unit cells along the y-axis and p the dimension of each unit cell. The results of this section were obtained for TE leaky-wave modes (H-plane). However, changing the equations of the impedances in the equivalent network yields the TM modes (E-plane).

4. ANTENNA PERFORMANCE

In order to validate the analytical and simulated results, a prototype of the proposed antenna of Figure 1 has been fabricated and tested. A picture of the physical device is shown in Figure 14.

Figure 14. Photograph of the proposed antenna.

Figure 15(a) shows a plot of measured reflection coefficient S_{11} as a function of frequency. For comparison and verification reasons, numerical simulations are also plotted using CST microwave studio, which is based on the FIT method. As can be observed, the operating frequency band of the proposed EBG antenna extends from 56 GHz to 63 GHz, corresponding to a bandwidth of 11.7%, wide enough to cover the unlicensed ISM band. Two resonances can be clearly seen: the first, in proximity of 57.5 GHz, is caused by the excitation of the TE_{11} mode of the DRA, and the second one, near 61 GHz, is caused by the slot radiation.

One can note that there is a frequency offset about 1.3 GHz, between the simulated and measured results, especially near the first resonance frequency (57.5 GHz). This shift is caused by the combined effect of manufacturing defects, connector and Rohacell foam losses. The measured and simulated EBG
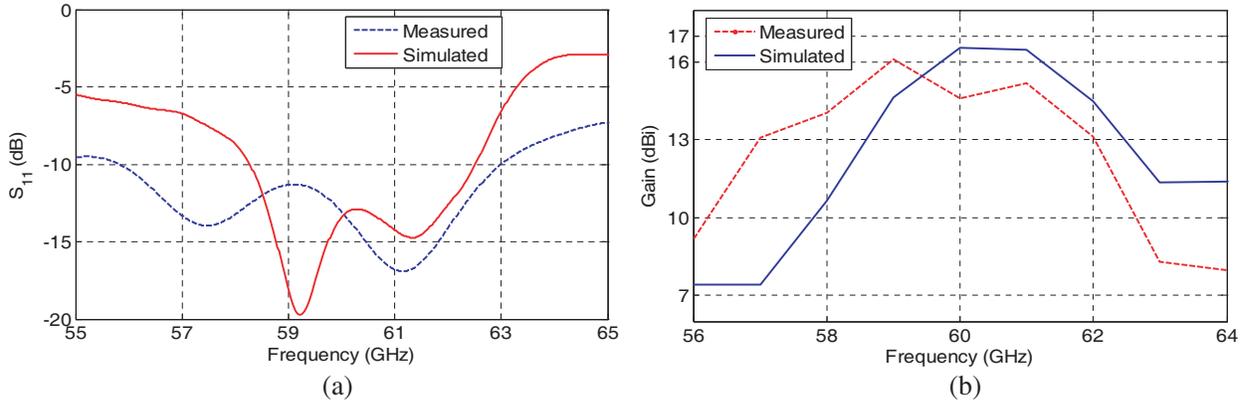
Figure 15. Measured and simulated: (a) Reflection coefficient S_{11}. (b) Gain.
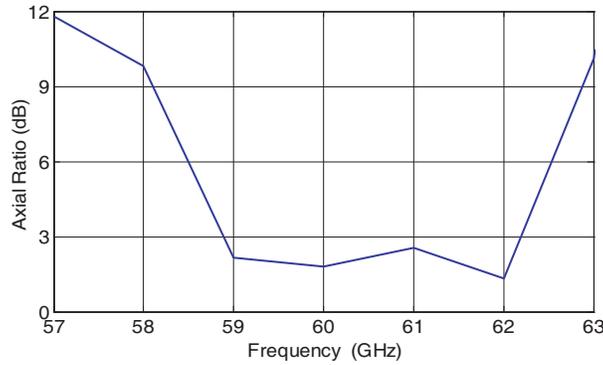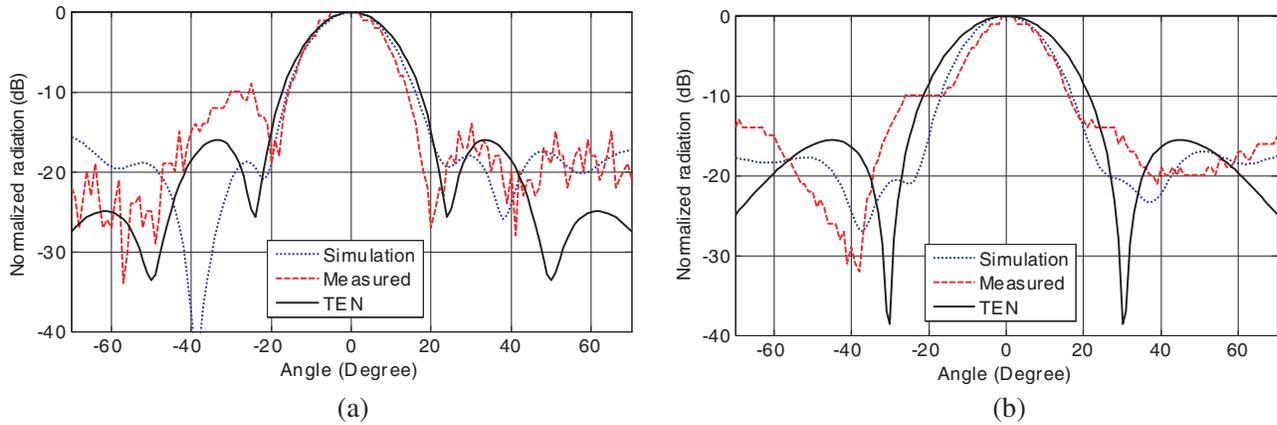

Figure 16. Simulated axial ratio (CST).

Figure 17. Measured, simulated and analyzed radiation pattern at 61 GHz. (a) E-plane. (b) H-plane.

antenna gains versus frequency are depicted in Figure 15(b). A peak gain of 16.7 dBi is achieved at 60 GHz, with a difference of 3 dB between the lowest and highest values, and the minimum gain is about 13.7 dBi at 62 GHz. It can also be pointed out that the gain shows good stability over the matching frequency band from 56 GHz to 63 GHz.

The 3-dB axial ratio, presented in Figure 16, exhibits a bandwidth of 5.4%, from 58.9 to 62.1 GHz, with a minimum about 1.3 dB around 62 GHz. The measured and simulated E and H plane radiation patterns at 61 GHz are shown in Figure 17(a) and Figure 17(b), respectively. These results show that

the proposed antenna has both highly directional main lobe and a high gain.

The maximum gain is achieved at 60 and 61 GHz where it reaches 16.7 dBi. These results correspond to the set objectives for a highly directional 60-GHz millimeter-wave antenna. It can also be observed that the measured radiation patterns are in good agreement with simulated and analysed ones.

Table 3 presents a summary performance comparison between the proposed EBG antenna and some other existing 60 GHz high gain antennas in terms of axial ratio band, bandwidth, maximum gain, efficiency and size. It can be concluded, from the results in the table, that the proposed EBG antenna not only has wider AR band, but also exhibits high gain, very high efficiency and broad impedance bandwidth. It also has the advantage that it can be easily fabricated if accuracy in geometry is preserved at all time.

Table 3. Performance comparison between the proposed antenna and some existing 60 GHz antennas.

	Axial Ratio	**Bandwidth**	**Gain (dBi)**	**Effeciency**	**Size (mm^3)**
[28]	Linear polarization	6.8% (58.7–62.7) GHz	14.6	76%	$30 \times 30 \times 3.39$
[29]	10% (56–62) GHz	12% (56.2–63.2) GHz	10.4	70%	$30 \times 20 \times 1.16$
[30]	17.9% (56.5–67.5) GHz	17.9% (56–67) GHz	14.2	85%	$10 \times 9.1 \times 0.787$
[31]	6.8% (58.6–62.7) GHz	6.7% (58–62) GHz	12.5	82%	$15 \times 10 \times 0.92$
Proposed in this paper	5.4% (58.9–62.1) GHz	11.7% (56–63) GHz	16.6 dBi	85%	$20 \times 25 \times 3$

5. CONCLUSION

This work presents a novel approach to improve the radiation properties of circular polarization EBG antennas using combination between dielectric resonator and FSS superstrate. The following contributions, in the area of Fabry-Perot leaky wave antenna, are presented.

The introduction of a new design of EBG antenna is characterised by a high gain and broadband circular polarization at millimeter-band, when a cross DRA is used to generate a circular polarization radiation. However, the DRA gain and bandwidth are improved by using an adequate FSS superstrate.

Very simple analytical formulas were developed to derive the radiation properties of the proposed antenna. The transmission line theory and transverse equivalent network (TEN) were used to predict the far-field radiation pattern for a dielectric resonator antenna covered with a superstrate. This technique has been found highly relevant for the analysis of the proposed antenna, and its major advantage is having very fast analysis speed compared to other simulation techniques and full-wave analysis which are inappropriately slow and require a lot of computational efforts.

A physical prototype has been manufactured using printed circuit technology, and a good agreement among analytical, numerical and measurements results is observed. A bandwidth in excess of 11.7% is achieved from 56 to 63 GHz, and a peak gain of 16.7 dBi is obtained at 60 GHz, mostly constant across all the operating band. The AR bandwidth was found to be about 5.4%, better than other cases with more sophisticated designs using sequential excitations. The proposed antenna with enhanced performance is suitable to be deployed in complex media such as underground communications systems.

REFERENCES

1. Guo, N., R. C. Qiu, S. S. Mo, and K. Takahashi, "60-GHz millimeter-wave radio: Principle, technology, and new results," *EURASIP Journal on Wireless Communications and Networking*, Vol. 2007, 2007.

2. Yildirim, F., A. S. Sadri, and H. Liu, "Polarization effects for indoor wireless communications at 60 GHz," *IEEE Communications Letters*, Vol. 12, No. 9, 660–662, Sep. 2008.

3. Rappaport, T. S., J. Murdock, and F. Gutierrez, "State of the art in 60-GHz integrated circuits and systems for wireless communications," *Proceedings of the IEEE*, Vol. 99, No. 8, 1390–1436, Aug. 2011.

4. Petosa, A. and A. Ittipiboon, "Dielectric resonator antennas: A historical review and the current state of the art," *IEEE Antennas Propag. Mag.*, Vol. 52, No. 5, 91–116, Oct. 2010.

5. Elkarkraoui, T., G. Y. Delisle, N. Hakem, and Y. Coulibaly, "High gain cross DRA antenna array for underground communications" *IEEE International Symposium on Antennas and Propagation*, Memphis, TN, USA, Jul. 6–12, 2014.

6. Vettikalladi, H., O. Lafond, and M. Himdi, "High-gain broad-band superstrate millimeter wave antenna for 60 GHz indoor communications," *5th ESA Workshop on Millimeter Wave Technology and Applications and 31st ESA Antenna Workshop at ESTEC*, Netherland, May 18–20, 2009.

7. Nasimuddin and K. P. Esselle, "A low-profile compact microwave antenna with high gain and wide bandwidth," *IEEE Trans. Antennas Propag.*, Vol. 55, No. 6, 1880–1883, Jun. 2007.

8. Petosa, A., A. Ittipiboon, Y. M. M. Antar, and D. Roscoe, "Recent advances in dielectric resonator antenna technology," *IEEE Antennas and Propagation Magazine*, Vol. 40, No. 3, 35–48, Jun. 1998.

9. Lee, M., S.-J. Kim, G. Kwon, C. M. Song, Y. Yang, K.-Y. Lee, and K. C. Hwang, "Circularly polarized semi-eccentric annular dielectric resonator antenna for X-band applications," *IEEE Antennas Wirel. Propag. Lett.*, Vol. 14, 1810–1813, 2015.

10. Chair, R., et al., "Aperture-fed wideband circularly polarized rectangular stair-shaped dielectric resonator antenna," *IEEE Trans. Antennas Propag.*, Vol. 54, No. 4, 1350–1352, Apr. 2006.

11. Sulaiman, M. I. and S. K. Khamas, "A singly fed rectangular dielectric resonator antenna with a wideband circular polarization," *IEEE Antennas Wireless Propag. Lett.*, Vol. 9, 615–618, Jun. 2010.

12. Kaklamani, D., "Full-wave analysis of a Fabry-Perot type resonator," *Journal of Electromagnetic Waves and Applications*, Vol. 13, No. 12, 1627–1634, 1999.

13. Huang, C.-Y., J.-Y. Wu, and K.-L. Wong, "Cross-slot-coupled microstrip antenna and dielectric resonator antenna for circular polarization," *IEEE Transactions on Antennas and Propagation*, Vol. 47, No. 4, 605–609, 1999.

14. Kumari, R. and R. Kumar, "Circular polarized dielectric resonator antenna: Design and developments," *Wireless Personal Communications*, Vol. 86, No. 2, 851–886, Jan. 2016.

15. Himdi, J. P. Daniel, and C. Terret, "Transmission line analysis of aperture coupled microstrip antenna," *Electronics Letters*, Vol. 25, No. 18, 1229–1230, Aug. 1989.

16. Baba, A. A., M. A. Zakariya, Z. Baharudin, M. Z. U. Rehman, M. F. Ain, and Z. A. Ahmad, "Equivalent lumped-element circuit of aperture and mutually coupled cylindrical dielectric resonator antenna array," *Progress In Electromagnetics Research C*, Vol. 45, 15–31, 2013.

17. Al-Jibouri, Y. B., H. Evans, E. Korolkiewicz, E. G. Lim, A. Sambell, and T. Viasits, "Cavity model of circularly polarised cross-aperture-coupled microstrip antenna," *IEE Proceedings: Microwaves, Antennas and Propagation*, Vol. 148, No. 3, 147–152, 2001.

18. Haneishi, M. and S. Yoshida, "A design method of circularly polarized rectangular microstrip antenna by one-feed point," *Electronics & communications in Japan*, Vol. 64, No. 4, 46–54, 1981.

19. Garg, R., B. Prakash, I. Bahl, and A. Ittipiboon, *Microstrip Antenna Design Handbook*, Artech House, 2001.

20. Ruan, Y.-F., Y.-X. Guo, and X.-Q. Shi, "Equivalent circuit model of a tri-resonance wideband dielectric resonator antenna," *Microwave and Optical Technology Letters*, Vol. 49, No. 6, 1427–1433, 2007.

21. Kishk, A. A., et al., "Numerical analysis of stacked dielectric resonator antennas excited by a coaxial probe for wideband applications," *IEEE Transactions on Antennas and Propagation*, Vol. 51, No. 8, 1996.

22. Feresidis, A. P. and J. C. Vardaxoglou, "High gain planar antenna using optimized partially reflective surfaces," *IEE Proceedings Microwaves, Antennas and Propagation*, Vol. 148, No. 6,

345–350, Dec. 2001.

23. Garcia-Vigueras, M., J. L. Gomez-Tornero, G. Goussetis, and A. R. WeilyY. J. Guo, "1D-leaky wave antenna employing parallel-plate waveguide loaded with PRS and HIS," *IEEE Transactions on Antennas and Propagation*, Vol. 59, No. 10, 3687–3694, 2011.

24. Zhao, T., D. R. Jackson, J. T. Williams, and A. A. Oliner, "General formulas for 2-D leaky-wave antennas," *IEEE Trans. Antennas Propag.*, Vol. 53, No. 11, 3525–3533, Nov. 2005.

25. García-Vigueras, M., J. L. Gómez-Tornero, G. Goussetis, D. Cañete-Rebenaque, and A. Álvarez-Melcón, "Software tool for the leaky-mode analysis of waveguides loaded with frequency selective surfaces," *European Conference on Antennas and Propagation (EuCAP)*, Berlin, Germany, Mar. 23–27, 2009.

26. Kosmas, P., A. P. Feresidis, and G. Goussetis, "Periodic FDTD analysis of a 2-D leaky-wave planar antenna based on dipole frequency selective surfaces," *IEEE Trans. Antennas Propag.*, Vol. 55, No. 7, 2006–2012, 2007.

27. Caloz, C. and T. Itoh, "Array factor approach of leaky/wave antennas and application to 1-D/2-D Composite Right/Left-Handed (CRLH) structures," *IEEE Microwave and Wireless Components Letters*, Vol. 14, No. 6, 274–276, Jun. 2004.

28. Vettikalladi, H., O. Lafond, and M. Himdi, "High-efficient and high-gain superstrate antenna for 60-GHz indoor communication," *IEEE Antennas Wireless Propagat. Lett.*, Vol. 8, 1422–1425, 2009.

29. Perron, A., T. A. Denidni, and A. R. Sebak, "Circularly polarized microstrip/elliptical dielectric ring resonator antenna for millimeter-wave applications," *IEEE Antennas Wireless Propag. Lett.*, Vol. 9, 783–786, Aug. 2010.

30. Bisharat, D. J., S. Liao, and Q. Xue, "Circularly-polarized planar aperture antenna for millimeter-wave application," *IEEE Trans. Antennas Propagation*, Vol. 63, No. 12, 5316–5324, 2015.

31. Guntupalli ,B. and K. Wu, "60-GHz circularly polarized antenna array made in low-cost fabrication process," *IEEE Antennas Wireless Propag. Lett.*, Vol. 13, 86–867, May 2014.